

# PERTURBATIONS OF INTERMEDIATE-MASS BLACK HOLES ON STELLAR ORBITS IN THE GALACTIC CENTER

ALESSIA GUALANDRIS AND DAVID MERRITT

Department of Physics and Center for Computational Relativity and Gravitation, Rochester Institute of Technology, 78 Lomb Memorial Drive, Rochester, NY  
Draft version September 9, 2021

## ABSTRACT

We study the short- and long-term effects of an intermediate mass black hole (IMBH) on the orbits of stars bound to the supermassive black hole (SMBH) at the center of the Milky Way. A regularized  $N$ -body code including post-Newtonian terms is used to carry out direct integrations of 19 stars in the S-star cluster for 10 Myr. The mass of the IMBH is assigned one of four values from  $400 M_{\odot}$  to  $4000 M_{\odot}$ , and its initial semi-major axis with respect to the SMBH is varied from 0.3–30 mpc, bracketing the radii at which inspiral of the IMBH is expected to stall. We consider two values for the eccentricity of the IMBH/SMBH binary,  $e = (0, 0.7)$ , and 12 values for the orientation of the binary’s plane. Changes at the level of  $\sim 1\%$  in the orbital elements of the S-stars could occur in just a few years if the IMBH is sufficiently massive. On time scales of 1 Myr or longer, the IMBH efficiently randomizes the eccentricities and orbital inclinations of the S-stars. Kozai oscillations are observed when the IMBH lies well outside the orbits of the stars. Perturbations from the IMBH can eject stars from the cluster, producing hypervelocity stars, and can also scatter stars into the SMBH; stars with high initial eccentricities are most likely to be affected in both cases. The distribution of S-star orbital elements is significantly altered from its currently-observed form by IMBHs with masses greater than  $\sim 10^3 M_{\odot}$  if the IMBH/SMBH semi-major axis lies in the range 3–10 mpc. We use these results to further constrain the allowed parameters of an IMBH/SMBH binary at the Galactic center.

*Subject headings:* Galaxy:center - stellar dynamics

## 1. INTRODUCTION

Near-infrared imaging and spectroscopy of the Galactic center indicate the presence of over 100 young massive stars in the inner parsec of the Milky Way. These belong to two distinct populations: (1) Outside the central arcsecond, a group of roughly 40 stars, mostly O and Wolf-Rayet stars with an estimated age of 6 Myr, move on approximately circular orbits in a thin and coherent stellar disk (Paumard et al. 2006) (2) Inside the central arcsecond, a group of 20 B-type stars (the S-stars) move on eccentric and randomly oriented orbits around the supermassive black hole (SMBH) (Ghez et al. 2003; Eisenhauer et al. 2005; Gillessen et al. 2009).

The existence of young massive stars so close to the SMBH is puzzling since tidal stresses from the SMBH are likely to suppress star formation in this region. If the S-stars formed at larger distances from Sgr A\* and were then transported inward, the migration would need to occur on a timescale of only a few Myr, given the apparent age of the stars. This constitutes the so-called *paradox of youth*.

Several scenarios have been proposed for the origin of the young stars in the Galactic center, including (i) rejuvenation of older stars due to physical collisions and/or tidal stripping in the vicinity of the SMBH (?Ghez et al. 2003), (ii) tidal disruption of binary stars on low angular momentum orbits (Gould & Quillen 2003; ?), (iii) in-situ formation from a fragmenting gas disk formed from an infalling molecular cloud (?Bonnell & Rice 2008), (iv) formation in a star cluster outside the central parsec and transportation by the inspiralling cluster (Gerhard 2001).

The spectra of the observed S-stars seem to indicate that they are ordinary B-type main-sequence stars, with no apparent evidence for an exotic history (Eisenhauer et al. 2005; Figer 2008). This would seem to exclude the rejuvenation scenario.

The binary disruption scenario postulates that the S-stars were once in binary systems on plunging orbits that were tidally disrupted by the SMBH, ejecting one star and leaving the other in an extremely eccentric orbit around the SMBH (Gould & Quillen 2003). This model requires an ad hoc reservoir of new binaries at large radii, a mechanism to scatter the stars onto plunging orbits (e.g. “massive perturbers”; Perets et al. (2007)), and an efficient mechanism to thermalize the eccentricities within the lifetime of the stars (e.g. “resonant relaxation” from stellar mass black holes; Perets et al. (2009)). Modified binary disruption scenarios in which the S-stars were born in a stellar disk have also been proposed (??).

The in-situ formation model assumes that an infalling molecular cloud interacts with the SMBH and forms a disk which then fragments and forms stars. This model successfully reproduces the observed properties of the disk stars (Bonnell & Rice 2008), including mild eccentricities and a top-heavy mass function. It however cannot account for the large eccentricities and random inclinations of the orbits of the S-stars.

Merritt et al. (2009) showed that these dynamical properties can be naturally explained by interaction of the stars with an intermediate mass black hole (IMBH) in the context of the inspiralling star cluster scenario. This model postulates that the S-stars were born in a star cluster at large enough distance from the SMBH that a giant molecular cloud could collapse and fragment. The new cluster then migrated inward due to dynamical friction, depositing stars along the way as the tidal force from the SMBH stripped them from the outer regions of the cluster (Gerhard 2001). If the cluster has by then formed an IMBH at its center, e.g. via the runaway merging scenario (Portegies Zwart & McMillan 2002), the cluster can remain bound and spiral inward for much longer before releasing all its component stars (Hansen & Milosavljević 2003), reaching distances of a few

arXiv:0905.4514v2 [astro-ph.GA] 14 Oct 2009

tens of milliparsecs before evolution of the IMBH/SMBH binary stalls (Baumgardt et al. 2006; Matsubayashi et al. 2007; Löckmann & Baumgardt 2008). Interactions with the same IMBH that brought the stars close to the SMBH can then randomize their orbital inclinations and thermalize their eccentricity distribution on timescales of  $\lesssim 1$  Myr (Merritt et al. 2009). The IMBH can also capture stars ejected from the cluster into a resonance and bring them close to the SMBH (?).

Whether or not the inspiralling star cluster model is correct, this work raises intriguing questions about the observable consequences of an IMBH that is currently imbedded in the S-star cluster. Are perturbations from an IMBH detectable on short (year-long) time scales, and if so, which of the S-stars are most likely to be affected? How stable is the cluster on time scales of order stellar lifetimes? Would an appreciable fraction of the stars be ejected from the Galactic center, or scattered into the SMBH, by the IMBH? What constraints can be placed on the physical parameters (mass, orbital elements) of a putative IMBH/SMBH binary given the need to conserve the observed distribution of orbital elements of the S-stars?

To address these questions, we have carried out a large set of high-accuracy  $N$ -body simulations, taking as our initial conditions the current positions and velocities of the  $\sim 20$  S-stars with well determined orbits, plus an additional massive particle representing the IMBH. In §2 we describe the initial conditions and the  $N$ -body methods. §3 discusses the short (few years) time scale effects on the observed stellar orbits. The longer term (Myr) behavior of the S-star cluster is described in §4. §5 summarizes our results and draws conclusions about the allowed parameter space for an IMBH/SMBH binary at the Galactic center.

## 2. INITIAL MODELS AND NUMERICAL METHODS

Our  $N$ -body models include a SMBH, an IMBH and a cluster of 19 S-stars. Gillessen et al. (2009) provide Keplerian elements for 28 stars, of which one (S111) appears to be unbound as a result of its large radial velocity, six (S66, S67, S83, S87, S96, S97) likely belong to the clockwise stellar disk (Genzel et al. 2003; Paumard et al. 2006) and one (S71) has a very long orbital period. The remaining stars have well defined or at least reliable orbits and exhibit essentially random orbital orientations. We determined positions and velocities at year 2008 AD for the 19 remaining stars from the classical elements<sup>1</sup> given in Table 1. The assumed SMBH mass is  $M_{\text{SMBH}} = 4.0 \times 10^6 M_{\odot}$  (Gillessen et al. 2009). The masses of the S-stars were set to  $10 M_{\odot}$  (e.g. Eisenhauer et al. 2005) except for star S-2 for which a value of  $20 M_{\odot}$  was adopted (Martins et al. 2008).

We considered four values of the IMBH mass,  $M_{\text{IMBH}} = (400, 1000, 2000, 4000) M_{\odot}$ , or  $q = M_{\text{SMBH}}/M_{\text{IMBH}} = (1, 2.5, 5, 10) \times 10^{-4}$ ; five values of the initial semi-major axis,  $a = (0.3, 1, 3, 10, 30)$  mpc; two values of the eccentricity,  $e = (0, 0.7)$ ; and twelve orientations of the IMBH/SMBH orbital plane, for a total of 480 initial models. The parameters of the simulations are summarized in Table 2.

<sup>1</sup> The orbital elements are defined as in Eisenhauer et al. (2005) and Paumard et al. (2006):  $a$  = semi-major axis;  $P$  = orbital period;  $e$  = eccentricity;  $i$  = inclination of the ascending node, i.e. angle between the orbital plane and the plane tangential to the celestial sphere ( $0^\circ < i < 90^\circ$  for direct counterclockwise projected rotation,  $90^\circ < i < 180^\circ$  for retrograde clockwise projected rotation);  $\Omega$  = position angle of the ascending node;  $\omega$  = longitude of periastron, i.e. the angle between the radius vector of the ascending node and that of the periastron counted from the node in the direction of the orbital motion.

TABLE 1  
S-STAR ORBITAL ELEMENTS

star	$P_{\text{orb}}$ (yr)	$a$ (mpc)	$e$	$i$ (deg)	$\Omega$ (deg)	$\omega$ (deg)
S1	128.0	19.462	0.483	120.1	341.3	116.9
S2	15.8	4.829	0.880	134.5	225.8	63.8
S4	58.2	11.523	0.407	77.8	257.9	316.9
S5	210.0	27.072	0.672	110.2	147.0	270.6
S6	119.0	18.601	0.898	86.5	84.0	126.2
S8	95.6	16.038	0.816	74.6	315.7	344.4
S9	62.3	12.054	0.867	80.4	145.7	229.7
S12	60.1	11.763	0.899	32.8	236.9	311.2
S13	56.3	11.263	0.471	27.8	72.0	247.5
S14	45.2	9.727	0.962	99.4	227.9	339.0
S17	62.0	12.019	0.370	96.3	187.2	318.7
S18	47.9	10.123	0.748	114.4	216.8	150.5
S19	323.0	36.140	0.863	74.6	343.7	157.0
S21	35.0	8.203	0.784	55.3	254.8	178.0
S24	444.0	44.677	0.941	106.6	3.0	290.1
S27	95.9	16.072	0.963	93.3	192.1	312.9
S29	85.1	14.839	0.936	127.0	157.3	346.3
S31	64.2	12.303	0.699	115.1	138.9	343.4
S33	95.0	15.967	0.731	44.5	82.7	326.9

TABLE 2  
PARAMETERS OF THE SIMULATIONS

Run $e = 0.0$	Run $e = 0.7$	$q$	$M_{\text{IMBH}}$ ( $M_{\odot}$ )	$a$ (mpc)	$P$ (yr)
1-12	241-252	$1.0 \times 10^{-4}$	400	0.3	0.243
13-24	253-264	$1.0 \times 10^{-4}$	400	1	1.481
25-36	265-276	$1.0 \times 10^{-4}$	400	3	7.696
37-48	277-288	$1.0 \times 10^{-4}$	400	10	46.837
49-60	289-300	$1.0 \times 10^{-4}$	400	30	243.373
61-72	301-312	$2.5 \times 10^{-4}$	1000	0.3	0.243
73-84	313-324	$2.5 \times 10^{-4}$	1000	1	1.481
85-96	325-336	$2.5 \times 10^{-4}$	1000	3	7.695
97-108	337-348	$2.5 \times 10^{-4}$	1000	10	46.834
109-120	349-360	$2.5 \times 10^{-4}$	1000	30	243.355
121-132	361-372	$5.0 \times 10^{-4}$	2000	0.3	0.243
133-144	373-384	$5.0 \times 10^{-4}$	2000	1	1.481
145-156	385-396	$5.0 \times 10^{-4}$	2000	3	7.695
157-168	397-408	$5.0 \times 10^{-4}$	2000	10	46.828
169-180	409-420	$5.0 \times 10^{-4}$	2000	30	243.324
181-192	421-432	$1.0 \times 10^{-3}$	4000	0.3	0.243
193-204	433-444	$1.0 \times 10^{-3}$	4000	1	1.480
205-216	445-456	$1.0 \times 10^{-3}$	4000	3	7.692
217-228	457-468	$1.0 \times 10^{-3}$	4000	10	46.816
229-240	469-480	$1.0 \times 10^{-3}$	4000	30	243.263

The orientations of the massive binary were not selected randomly but rather were distributed uniformly on a grid. The surface of a sphere can be uniquely tessellated by means of 12 regular pentagons, the centers of which form a regular dodecahedron inscribed in the sphere. We determined the centers of the pentagons and transformed the coordinates of the points into inclination  $i$  and longitude of ascending node  $\Omega$  of the IMBH/SMBH orbit. We then rotated the points by an arbitrary angle to avoid chance superpositions with the S-star orbital inclinations. The resulting distribution of angular momentum vectors on the plane of the sky is shown in Figure 1; the values of the 12 angles are given in Table 3.

We followed the evolution of each 21-body system for a time corresponding to 10 Myr using the AR-CHAIN code

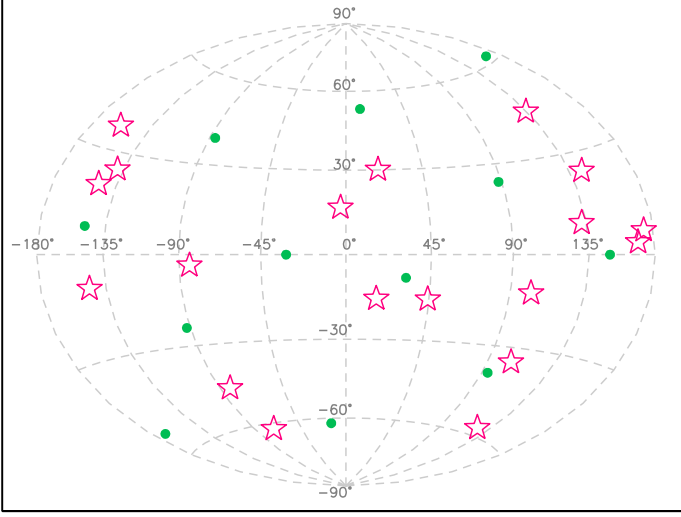


FIG. 1.— Directions of the angular momentum vector of the 19 S-stars (stars) and of the 12 possible orientations of the IMBH/SMBH orbit (circles). In this all-sky map, the vertical dimension refers to the inclination  $i$  of the orbit and the horizontal dimension to the longitude of the ascending node  $\Omega$ , as defined in Eisenhauer et al. (2005) and Gillessen et al. (2009). The Galactic plane lies at  $i = 0^\circ$ ,  $\Omega = -31.4^\circ$ .

TABLE 3  
GRID OF IMBH/SMBH ORBITAL INCLINATIONS

number	$i$ (deg)	$\Omega$ (deg)
1	90.0	31.49
2	129.21	86.17
3	50.79	266.17
4	90.0	211.49
5	27.97	14.14
6	81.95	328.25
7	98.05	148.23
8	152.03	194.14
9	66.07	92.05
10	37.09	169.12
11	142.91	349.12
12	113.93	272.05

(Mikkola & Merritt 2008), a recent implementation of the algorithmic regularization method that is able to reproduce the motion of tight binaries for long periods of time with extremely high precision. The code combines the use of the chain structure, introduced originally by Mikkola & Aarseth (1993), with a new time-transformation to avoid singularities and achieve high precision for arbitrary mass ratios. Integrations were carried out on two computer clusters at the Center for Computational Relativity and Gravitation at the Rochester Institute of Technology: `gravitySimulator` (Harfst et al. 2007) and `newHorizons`<sup>2</sup>, and on one computer cluster hosted by the Research Computing group at the same institution.

The AR-CHAIN code also includes post-Newtonian corrections to the accelerations up to order PN2.5. This is necessary due to the fact that the general relativistic precession timescale

<sup>2</sup> <http://ccrg.rit.edu/facilities>

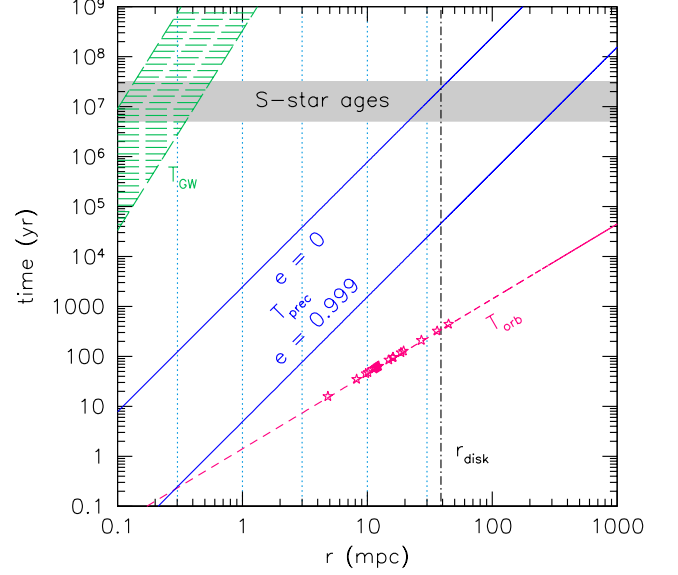


FIG. 2.— Relevant timescales for the S-stars and the IMBH as a function of distance from the SMBH:  $T_{\text{orb}}$  orbital period (dashed line); star symbols are the S-stars,  $T_{\text{prec}}$  relativistic precession timescale (solid lines) for eccentricities  $e = 0$  and  $e = 0.999$ ,  $T_{\text{GW}}$  gravitational wave emission timescale for  $M_{\text{IMBH}} = 400 - 4000 M_\odot$  and  $e = 0 - 0.7$  (dashed region). The vertical dotted lines represent the adopted values for the black hole binary initial separation. The filled grey region indicates the estimated ages of the S-stars. The vertical dotted-dashed line represents the outer edge of the disk of massive stars.

(accounted for by the PN1 and PN2 terms)

$$T_{\text{PR}} = \frac{2\pi c^2 (1 - e^2) a^{5/2}}{3(GM_{\text{SMBH}})^{3/2}} \simeq 8.2 \times 10^5 \text{yr} \left( \frac{a}{10 \text{ mpc}} \right)^{5/2} \left( \frac{4 \times 10^6 M_\odot}{M_{\text{SMBH}}} \right)^{3/2} (1 - e^2) \quad (1)$$

is generally much shorter than the integration time (see also Fig. 2). The energy loss due to emission of gravitational waves (accounted for by the PN2.5 term) occurs on a timescale

$$T_{\text{GW}} = \frac{5}{256F(e)} \frac{c^5}{G^3} \frac{a^4}{\mu(M_{\text{SMBH}} + M_{\text{IMBH}})^2} \simeq \frac{3.6 \times 10^{10} \text{yr}}{F(e)} \left( \frac{a}{10 \text{ mpc}} \right)^4 \left( \frac{4 \times 10^6 M_\odot}{M_{\text{SMBH}}} \right) \left( \frac{10^3 M_\odot}{M_{\text{IMBH}}} \right) \times \left( \frac{4 \times 10^6 M_\odot}{M_{\text{SMBH}} + M_{\text{IMBH}}} \right) \quad (2)$$

where

$$F(e) = (1 - e^2)^{-7/2} \left( 1 + \frac{73}{24} e^2 + \frac{37}{96} e^4 \right) \quad (3)$$

and

$$\mu = \frac{M_{\text{SMBH}} * M_{\text{IMBH}}}{M_{\text{SMBH}} + M_{\text{IMBH}}} \approx q M_{\text{IMBH}}. \quad (4)$$

This is typically  $\gtrsim 10 \text{ Myr}$  (see Fig. 2), implying that the orbit of the IMBH does not evolve appreciably over the integration time. The only exception is the set of runs with  $q = 10^{-3}$ ,  $a = 0.3 \text{ mpc}$  and  $e = 0.7$ , for which  $T_{\text{GW}} \lesssim 3 \text{ Myr}$ .

Some relevant timescales for the S-stars and the IMBH are shown in Figure 2. One timescale that is not illustrated there is that associated with dynamical friction of the IMBH against the background stars. Assuming a circular orbit for the IMBH, the frictional drag is given by (Binney & Tremaine 1987, Eq.7-18)

$$F = -\frac{4\pi \ln \Lambda G^2 \rho(r) M_{\text{IMBH}}^2}{v_c^2} \left( \text{erf}(X) - \frac{2X}{\sqrt{\pi}} e^{-X^2} \right) \quad (5)$$

where  $\rho(r)$  is the background stellar density,  $\ln \Lambda$  the Coulomb logarithm and  $X = v_c / \sqrt{2} \sigma$  is the ratio of the IMBH velocity to the one-dimensional velocity dispersion  $\sigma$ . The rate of change of the angular momentum  $L = r v_c = \sqrt{GM_{\text{SMBH}}} r$  can be written as  $dL/dt = F r / M_{\text{IMBH}}$ . Assuming  $X = 1$ , this implies

$$r^{-5/2} \frac{dr}{dt} = -3.4\pi \ln \Lambda \sqrt{G} \frac{M_{\text{IMBH}}}{M_{\text{SMBH}}^{3/2}} \rho(r) \quad (6)$$

The dynamical friction timescale is then

$$T_{\text{DF}} = \left| \frac{1}{r} \frac{dr}{dt} \right|^{-1} = \frac{1}{3.4\pi \ln \Lambda \sqrt{G}} \frac{M_{\text{SMBH}}^{3/2} r^{-3/2}}{M_{\text{IMBH}} \rho(r)} \\ \simeq 2 \times 10^7 \text{ yr} \left( \frac{M_{\text{SMBH}}}{4 \times 10^6 M_{\odot}} \right)^{3/2} \left( \frac{10^3 M_{\odot}}{M_{\text{IMBH}}} \right) \left( \frac{10^5 M_{\odot} \text{ pc}^{-3}}{\rho} \right) \left( \frac{r}{\text{pc}} \right)^{3/2}$$

having taken  $\ln \Lambda = 6.6$  (Spinnato et al. 2003).

Since our  $N$ -body models include only a fraction of the stellar mass in this region, the IMBH experiences essentially no dynamical friction. This may, or may not, be an accurate representation of what would actually happen at the Galactic center. Recent observations (??) raise questions about the existence of a density cusp in the observed stellar population within the central parsec: Number counts of the late-type (old) stars suggest a density that *drops* inside of  $\sim 0.5$  pc. Proper-motion data (?) are also consistent with a mass density that falls toward SgrA\*. Even if a density cusp were present initially, an inspiralling IMBH tends to displace the background stars and create a low-density core on a scale of  $\sim 0.1$  pc (Baumgardt et al. 2006). The absence of dynamical friction in our simulations may therefore be a reasonable approximation.

By ignoring the possibility of a density cusp, we also exclude the other dynamical effects that would accompany a high density of background stars, including cusp-induced precession of the orbits; damping of Kozai oscillations; and ejection of S-stars by close interactions with stellar remnants.

### 3. RESULTS: SHORT-TERM EVOLUTION

One motivation for basing our  $N$ -body models on the actual S-star orbits is that we are able to make quantitative statements about how these orbits would evolve in the near future.

While a close encounter of the IMBH with a star can produce a sudden large change in the star's velocity, such encounters are relatively rare, and the evolution of the star's trajectory is better described in terms of the change with time of its orbital elements. Figures 3 and 4 summarize the evolution of the orbit of star S1 over the next 1000 yr in each of the 120 integrations corresponding to  $q = 10^{-3}$ . We have plotted the changes in  $a$ ,  $e$  and  $\theta$  with respect to their values in the year 2008; here  $\theta$  is the angle in radians between the star's orbital angular momentum vector at the two times.

The IMBH lies completely inside the orbit of S1 in the top three rows of Figure 3 and 4. In these runs, the star's orbital elements (which are computed with respect to the instantaneous position and velocity of the SMBH) are found to oscillate due to the movement of the SMBH in response to the IMBH. Oscillation on both the (short) timescale of the IMBH/SMBH orbit, and the (longer) timescale of the star's orbit, can be seen. The amplitude of these oscillations is greatly reduced when the orbital elements are computed with respect to the center of mass of the IMBH/SMBH binary; there is almost no true evolution of the star's orbit on these time scales.

When the IMBH's orbit is larger than that of the star, oscillatory changes in the star's orbit still take place on the (now shorter) timescale of its own orbit, but in addition there are stepwise changes that occur roughly once per orbit of the IMBH, when it comes closest to the star. The latter changes are similar in magnitude for the circular and eccentric binaries, but in the latter case, changes in S1's orbit are less dependent on the binary's orientation.

We chose to place the IMBH at apoastron at the start of the integrations, and this choice determined the time of first and subsequent "close encounters" with each star. This is clear in the lower panels of Figs. 3 and 4, where the IMBH orbit has a longer period than that of S1. Had we varied the argument of periastron for the IMBH, the jumps in S1's orbital elements would have taken place at different times with respect to 2008. These jumps can be significant, e.g. as large as  $\sim 30$  arc minutes in the case of  $\theta$ . However based on the figures, the a priori chance of such a jump occurring during any short ( $\sim$  years-long) interval of time is small.

According to Gillessen et al. (2009), the errors in the observationally determined values of  $a$ ,  $e$  and  $\theta$  for S1 are  $\sim 5\%$ ,  $\sim 0.03$  and  $\sim 0.01$  radians respectively. Figures 3 and 4 suggest that short-term ( $\sim$  few years) changes in the semi-major axis might rise above the measurement uncertainties for IMBH/SMBH binaries with  $q \approx 10^{-3}$  and  $a \lesssim 1$  mpc ( $e = 0$ ) and  $a \lesssim 3$  mpc ( $e = 0.7$ ). Changes in  $e$  and  $\theta$  might barely be detectable on the same timescale for  $a \lesssim 0.3$  mpc.

## 4. RESULTS: LONG-TERM EVOLUTION

The perturbations exerted by the IMBH induce changes in the orbital elements of the stars. In particular, the presence of an IMBH has the following effects: (i) randomization of the inclinations of the stars, (ii) ejection of stars from the region, (iii) scattering of stars onto plunging orbits that result in tidal disruption in the SMBH's tidal field (iv) secular effects like Kozai cycles.

### 4.1. Randomization of the orbital planes

The randomization of the orbital planes has been shown by Merritt et al. (2009) to be efficient for IMBH masses larger than  $\sim 1500 M_{\odot}$  and eccentricities larger than  $\sim 0.5$ . In these cases, a thin corotating disk of stars was converted into an isotropic distribution in just  $\sim 1$  Myr. In this work, we consider a population of stars that are already approximately isotropic at the beginning of the simulations. Nonetheless, the IMBH acts to randomize the orbital planes of the stars so that the angular momentum vectors can point to very different directions at the end of the 10 Myr evolution, as can be seen in Figure 5 in the case of star S9.

### 4.2. Ejections

Perturbations from the IMBH can also result in ejections of stars from the region. While ejections can be produced by

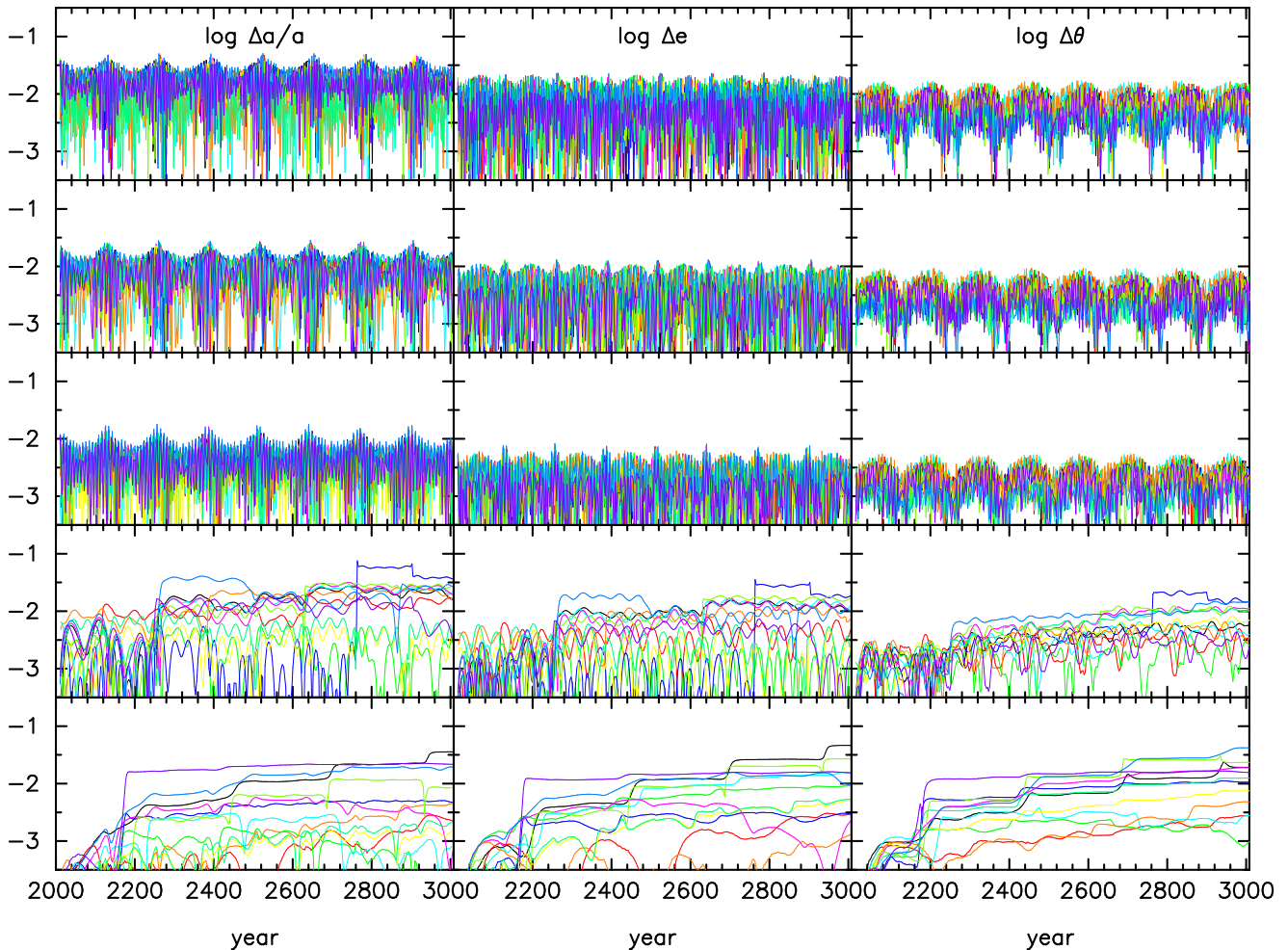


FIG. 3.— Changes over the initial 1000 years (i.e. from 2008 to 3008) of the orbital elements of star S1, in runs with  $q = 10^{-3}$ , a circular IMBH orbit, and five different values of  $a_{\text{IMBH}}$ , from 0.3 mpc (top) to 30 mpc (bottom). Different colors denote the 12 different orientations of the IMBH/SMBH orbital plane.

close encounters with the IMBH, the majority of the events are due to slow but steady increase in a star’s eccentricity, until eventually the star becomes unbound to the SMBH. We expect the probability of ejection to depend on both the stellar and the IMBH orbital parameters. Figure 6 shows the average number of escapers produced in any simulation with given mass ratio  $q = M_{\text{IMBH}}/M_{\text{SMBH}}$  and semi-major axis  $a$  of the binary black hole. We find that most of the ejections occur for large mass ratios and for separations comparable to the typical distances of the S-stars. These parameters maximize the strength of the perturbations, which tend to alter the eccentricity of the star. A circular and an eccentric binary seem to produce approximately the same number of escapers.

Stars with initially large eccentricity are more susceptible to perturbations and therefore more likely to be ejected, as shown in Figure 7. In particular, with  $e = 0.96$  star S14 is the one which experiences the most ejections.

Extrapolating the results obtained for the S-stars sample to the real Galactic center population (assuming a total of  $10^4$  stars in the same region) we obtain an ejection rate  $\mathcal{R} \sim 1.8 \times 10^{-4} \text{ yr}^{-1}$ .

#### 4.2.1. Survival time

Since stars can become unbound from the SMBH and escape the region monitored by observations, it is interesting to

study the “survival” probability for the S-stars, for a given set of orbital parameters. We estimate the mean time until ejection  $T_{ej}$  for individual stars for a given set of binary parameters. Since not all stars are ejected before the end of the simulation, an average of the ejection time over the cases where ejection occurs would yield a lower limit to  $T_{ej}$ . The problem of estimating the lifetime of a population given a discrete set of events within a finite time is called “survival analysis under censoring”, where censoring refers to the fact that at the end of the simulation only a fraction of the stars have a measured time of ejection. We therefore apply a maximum likelihood statistical analysis to our sample of censored data and compute the mean ejection time for each star and for a given set of binary parameters by averaging over the 12 runs which correspond to the different binary orientations in the sky. We define  $N_e$  the number of ejection events experienced by a star by the end of the simulations at time  $T$  and  $N_c$  the number of non ejections. If  $t_i, i = 0 \dots N_e$  are the ejection times for the events, the mean ejection time for a given star is

$$T_{ej} = \frac{1}{N_e} \sum_{i=0}^{N_e} t_i + \frac{N_c}{N_e} T \quad (9)$$

The results are shown in Figure 8 for all stars and provide a quantitative estimate of the probability of ejection for in-

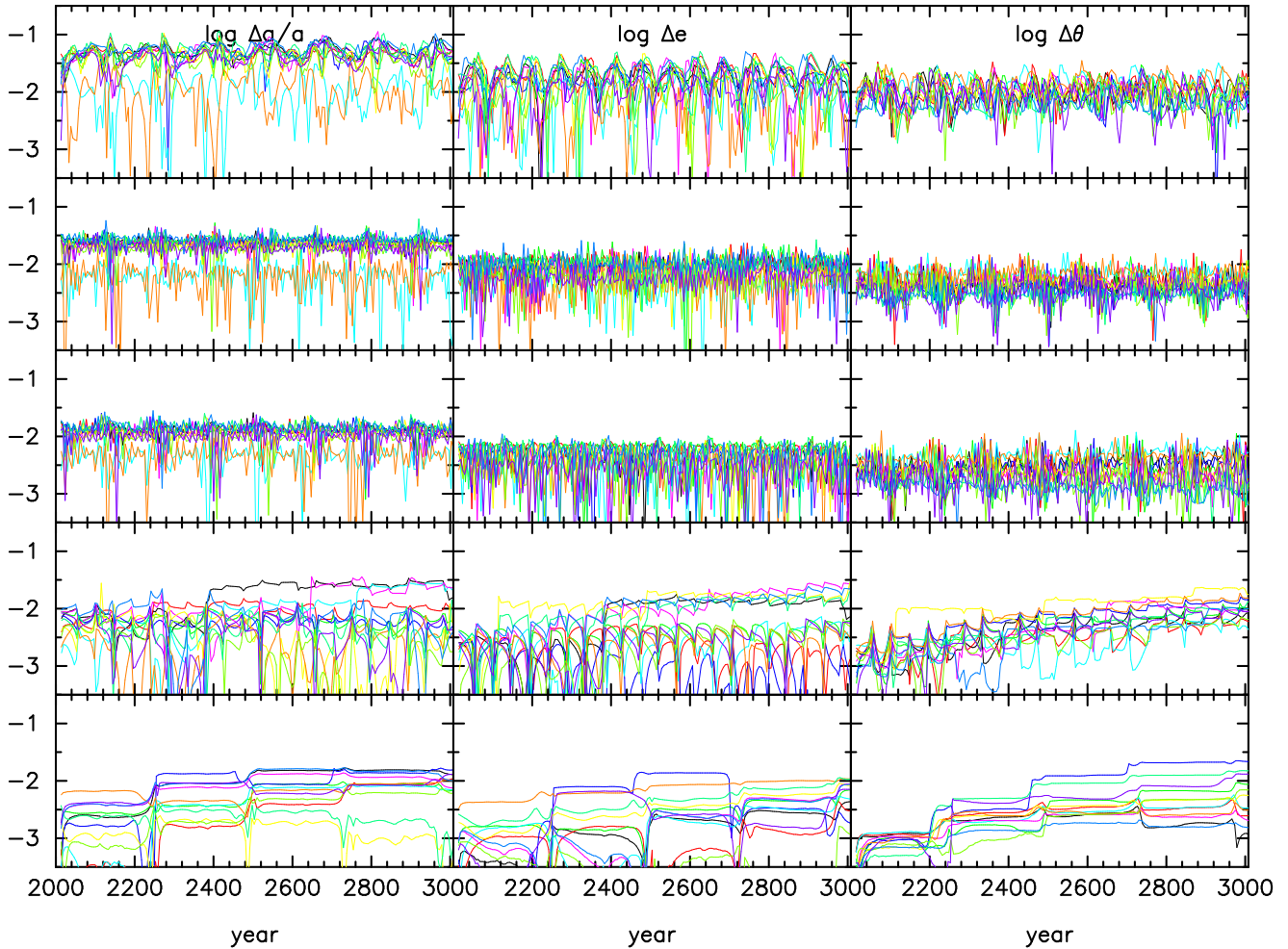


FIG. 4.— Like Fig. 3, but for runs with the eccentric IMBH/SMBH binary.

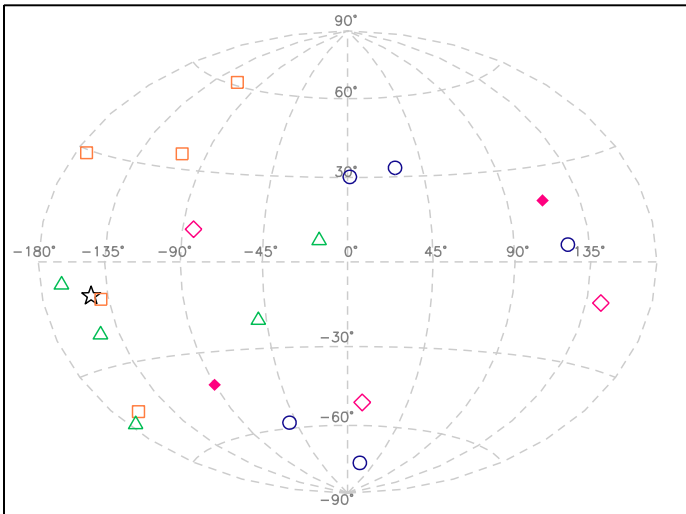


FIG. 5.— Orientation of the orbital plane of star S9 as currently observed (star) and at the end of the simulations (empty symbols if bound star; full symbols if unbound star). Different symbols are for different binary mass ratios:  $q = 1.0 \times 10^{-4}$  (circles),  $q = 2.5 \times 10^{-4}$  (squares),  $q = 5.0 \times 10^{-4}$  (triangles),  $q = 1.0 \times 10^{-3}$  (diamonds).

dividual stars taking into account both the orbital properties of the stars and of the IMBH. The mean time to ejection is  $\lesssim 10^7$  yr in the case of binaries with  $q \gtrsim 5.0 \times 10^{-4}$  and  $3 \text{ mpc} \lesssim a \lesssim 10 \text{ mpc}$ . Similarly to Figure 7, stars with large eccentricities have the shortest  $T_{\text{ej}}$ .

#### 4.2.2. Hypervelocity stars

A fraction of the escapers produced during the evolution can be ejected with large enough velocity to become unbound to the Galaxy. Such stars would be detected in the Galactic halo as hypervelocity stars (HVSs) (Brown et al. 2005). Assuming a threshold velocity of  $700 \text{ km s}^{-1}$  for escaping the Milky Way's potential, we find that about 15% of all the escapers become hypervelocity stars. The average velocity for the full sample of escapers is  $\sim 350 \text{ km s}^{-1}$  for the circular binary and  $\sim 400 \text{ km s}^{-1}$  for the eccentric binary, while for the sample of HVSs the mean is  $\sim 1450 \text{ km s}^{-1}$  and  $\sim 1550 \text{ km s}^{-1}$  respectively. This is consistent with the theoretical estimate by Yu & Tremaine (2003)

$$V_{\text{ej}} \simeq \sqrt{\frac{3.2 G M_{\text{SMBH}} M_{\text{IMBH}}}{(M_{\text{SMBH}} + M_{\text{IMBH}}) a}} \quad (10)$$

$$\sim 2.3 \times 10^3 \text{ km s}^{-1} \left(\frac{\nu}{0.1}\right)^{1/2} \left(\frac{\text{mpc}}{a}\right)^{1/2} \left(\frac{M_{\text{SMBH}}}{4 \times 10^6 M_{\odot}}\right)^{1/2} \quad (11)$$

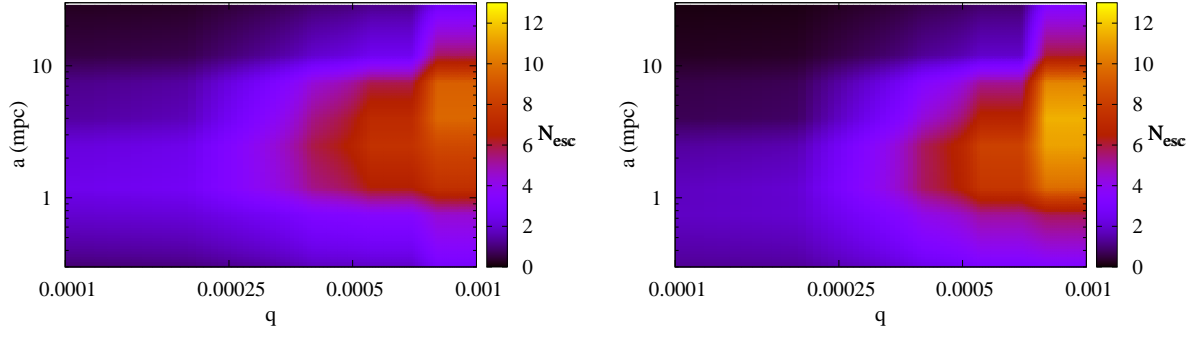


FIG. 6.— Average number of ejected stars as a function of the black hole binary parameters, in the case of an initially circular (left) and eccentric (right) binary.

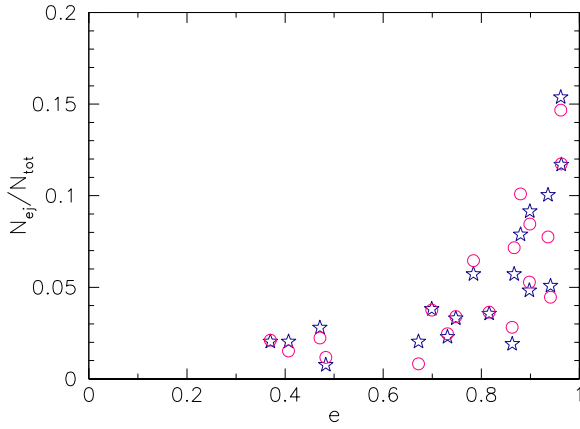


FIG. 7.— Fraction of ejections experienced by each S-star as a function of the star's initial eccentricity in the case of a circular (stars) and eccentric (circles) binary.

where  $\nu = \frac{M_{\text{IMBH}}}{M_{\text{SMBH}} + M_{\text{IMBH}}}$ . The distribution of ejection velocities for escapers has a peak around  $\sim 100 \text{ km s}^{-1}$  and shows a long tail toward high velocities (up to several thousand  $\text{km s}^{-1}$ ).

#### 4.3. Tidal captures and mergers

Interactions with the IMBH can also drive stars to be captured (either tidally disrupted or accreted) by the massive black hole. The Schwarzschild radius for the Milky Way black hole is given by

$$R_S = \frac{2GM_{\text{SMBH}}}{c^2} \sim 3.8 \times 10^{-7} \text{ pc} \quad (12)$$

while the tidal radius for a solar type main-sequence star is

$$R_t = R_* \left( \frac{\eta^2 M_{\text{SMBH}}}{m_*} \right)^{1/3} \quad (13)$$

$$\sim 3.6 \times 10^{-6} \text{ pc} \left( \frac{M_{\text{SMBH}}}{4 \times 10^6 M_\odot} \right)^{1/3} \left( \frac{M_\odot}{m_*} \right)^{1/3} \left( \frac{R_*}{R_\odot} \right) \eta^{2/3}$$

For simplicity we set the capture radius for all stars to  $R_t = 3R_S$ . When a star approaches the SMBH within such distance, it is merged with the black hole. The mass of the star is added to that of the black hole and new positions and velocities are computed. Mergers occur when stars are scattered

onto plunging orbits, and are therefore rare events in the simulations. The total number of captures (out of 240 integrations) experienced by the stars is 13 and 58 (corresponding to a probability of about 5 and 25%) for the circular and eccentric case, respectively, indicating that an eccentric binary is more likely to lead to a capture event. Large eccentricity stars are more likely to be tidally disrupted by the SMBH, as can be seen in Figure 9.

Simulations with  $q = 10^{-3}$ ,  $a = 0.3 \text{ mpc}$  and  $e = 0.7$  have the shortest time for emission of gravitational waves, namely  $\sim 2.7 \text{ Myr}$  (see Eq. 2). For this choice of parameters, the orbit of the IMBH decays due to energy loss, which is correctly implemented in the code, until the two black holes coalesce. From this point on, the integration is carried on with only one black hole.

#### 4.4. Kozai oscillations

The presence of an IMBH outside the orbits of the S-stars results in perturbations on the inner stellar orbits. In particular, Kozai oscillations (Kozai 1962) can be induced in the stellar orbits if the SMBH - star - IMBH system can be regarded as a hierarchical triple with a large inclination between the inner and the outer orbit. If the relative inclination is large, the time-averaged tidal force exerted on the inner binary produces variations in the eccentricity  $e_{\text{inn}}$ , inclination  $j$  and argument of pericenter  $\omega$ . The variations are such that the quantity

$$h = (1 - e^2) \cos^2(j), \quad (15)$$

also known as *Kozai integral*, is conserved. This is proportional to the component of the inner angular momentum perpendicular to the outer orbit. The semi-major axis of the inner and outer orbits can have periodic perturbations but no long-term evolution, so they can be assumed to be roughly constant. While the evolution of the eccentricity and inclination is always oscillatory, the argument of pericenter may either oscillate (*libration*) or circulate (*circulation*). In either case the periodic oscillations in  $e_{\text{inn}}$  and  $j$  are often called *Kozai cycles*. Remarkably, the variations in  $j$ ,  $e_{\text{inn}}$  and  $\omega$  do not depend on the masses of the stars or the dimensions of the orbits. These affect only the timescale of the effect and not its size.

The characteristic time-scale for Kozai oscillations is given by (Heggie & Hut 2003; Kinoshita & Nakai 2007)

$$T_K = \frac{4\mathcal{K}}{3\sqrt{6}\pi} \frac{P_{\text{out}}^2}{P_{\text{inn}}} \frac{M_{\text{SMBH}} + m_*}{M_{\text{IMBH}}} (1 - e_{\text{out}}^2)^{3/2} \quad (16)$$

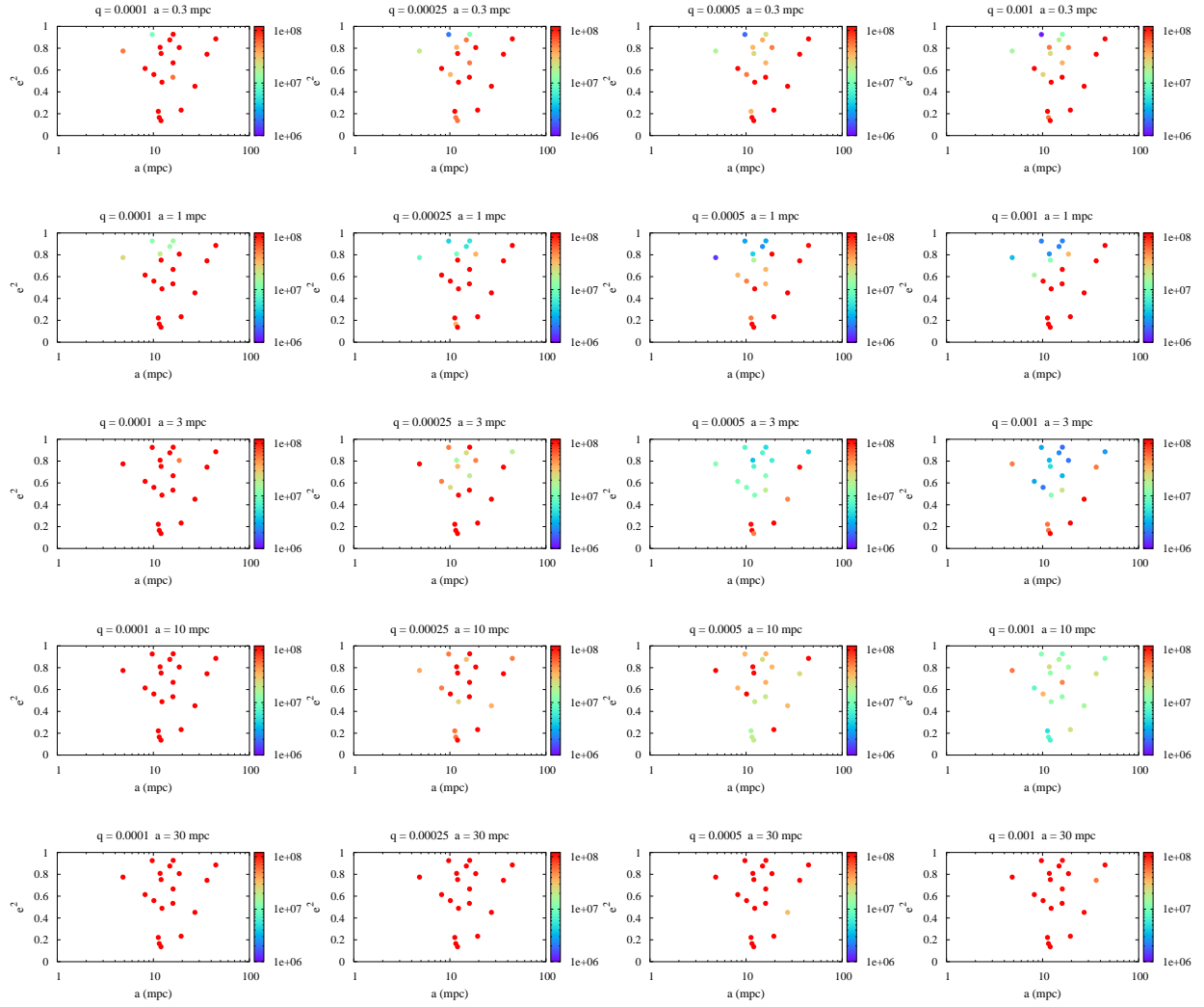


FIG. 8.— Mean time until ejection for all the stars as a function of the binary orbital parameters.

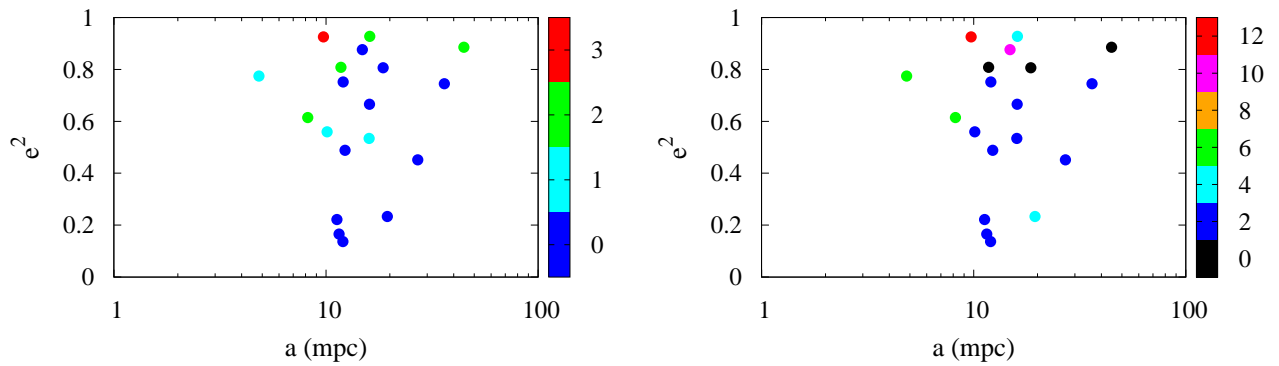


FIG. 9.— Total number of mergers experienced by the individual stars as a function of their orbital parameters. Left: initially circular binary. Right: Initially eccentric binary.



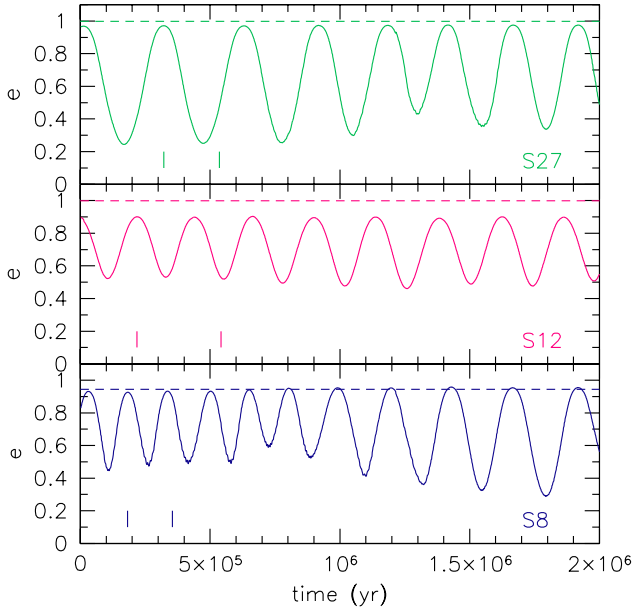


FIG. 10.— Eccentricity evolution of stars S8, S12 and S27 in a run with  $M_{\text{IMBH}} = 4000 M_{\odot}$ ,  $a = 30 \text{ mpc}$ ,  $e = 0$  and with relative inclinations of  $j = 58^{\circ}$ ,  $86^{\circ}$ ,  $79^{\circ}$ , respectively. Horizontal dashed lines represent the value of the maximum eccentricity predicted for the Kozai mechanism while the solid vertical lines indicate the Kozai timescale.

where  $P_{\text{inn}}$  and  $P_{\text{out}}$  are the period of the inner and outer binary and  $\mathcal{K}$  is a numerical coefficient which depends only on the initial values of  $j$ ,  $e_{\text{inn}}$  and  $\omega$ .

The maximum eccentricity  $e_{\text{max}}$  attained by the inner binary is also a function of the initial values of  $j$ ,  $e_{\text{inn}}$  and  $\omega$  only. In the case of a circular inner binary,  $e_{\text{max}}$  only depends on the initial relative inclination.

Kozai oscillations can be damped by general relativistic precession.

Three conditions must be satisfied in order for the Kozai mechanism to operate in our simulations: (i) the IMBH orbit must lie outside the orbits of the S-stars, so that the three body system can be regarded as a hierarchical triple. Whenever the inner and outer orbital periods are well separated, Eq. 16 accurately predicts the time scale for the oscillations in the eccentricity. The amplitude of the oscillations can also be predicted from the initial parameters (Kinoshita & Nakai 2007). (ii) The inner and outer orbits must be sufficiently inclined with respect to each other. (iii) The period of the Kozai oscillations must be shorter than the age of the system and shorter than that of any other mechanism that might wash out the oscillations, e.g. relativistic precession.

We therefore expect to observe Kozai oscillations in the simulations with large  $a_{\text{out}}/a_{\text{inn}}$  (like the runs with initial binary separation  $a = 30 \text{ mpc}$ ) for those stars whose orbits are significantly inclined with respect to the SMBH/IMBH plane and with a long precession time scale. Also, the timescale for oscillations will be shorter in the runs with the largest IMBH mass ( $q = 10^{-3}$ ).

Figure 10 shows the evolution of the eccentricity for three stars which exhibit Kozai oscillations in a run with  $M_{\text{IMBH}} = 4000 M_{\odot}$ ,  $a = 30 \text{ mpc}$  and  $e = 0$ . The predicted values of the maximum eccentricity and of the Kozai timescale are also shown. The agreement is satisfactory in all cases. As expected, the semi-major axis of the inner orbit remains constant

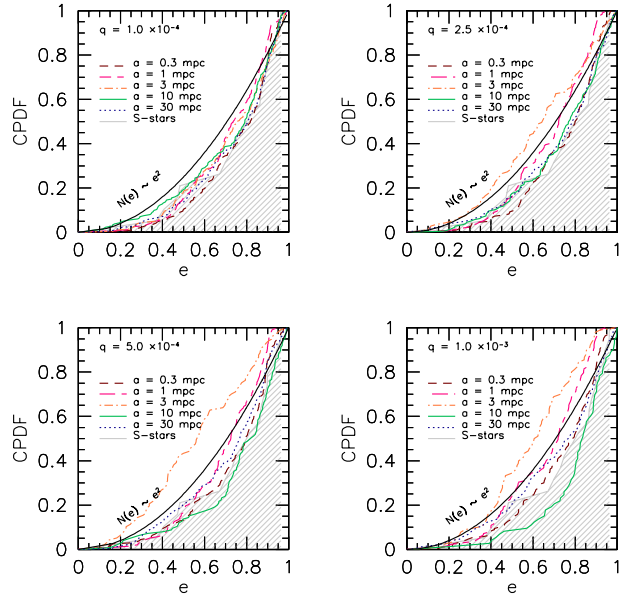


FIG. 11.— Cumulative distribution function for the eccentricities of the S-stars after 10 Myr of evolution in the case of a circular binary. Different lines are for different values of the binary semi-major axis. Each line is an average over the 12 different simulations with different IMBH 3D orientation with respect to the stars. The four panels refer to the four different values of the binary mass ratio. The shaded area represents the initial distribution of the stars. The  $N(e) \sim e^2$  line corresponds to an isotropic distribution of eccentricities.

and  $h$  is conserved while the eccentricity and the inclination oscillate.

## 5. EFFECTS ON THE OBSERVED POPULATION

The perturbations described in the previous section act to modify the orbital elements of the stars. Figure 11 shows the cumulative distribution for the eccentricities of the S-stars that remain bound at the end of the simulations. The four panels refer to the four different values of the binary mass ratio. The distributions for  $M_{\text{IMBH}} = 400 - 1000 M_{\odot}$  are consistent with an isotropic distribution of eccentricities  $P(e) \sim e$  for all values of the binary semi-major axis. For larger black hole masses ( $M_{\text{IMBH}} = 2000 - 4000 M_{\odot}$ ), however, only very small ( $a = 0.3 - 1 \text{ mpc}$ ) or very large ( $a \geq 30 \text{ mpc}$ ) semi-major axes result in final distributions consistent with observations. Results from an eccentric black hole binary appear qualitatively similar. The figure suggests that the IMBH exerts the largest perturbations at separations of order  $a \sim 3 - 10 \text{ mpc}$ , which is comparable to the semi-major axes of the S-stars. A close inspection of Figure 11 reveals that the final distributions can deviate from the observed one in two ways: either the final curve lies above the observed distribution, as is the case for  $a = 1 - 3 \text{ mpc}$ , or it lies below the observed distribution, as in the case of  $a = 10 \text{ mpc}$ . The reason for such distinctively different behavior is the competition between two effects of the IMBH perturbations: the tendency to increase the mean eccentricity of the population and the removal of stars from the population once they become unbound. The former process tends to move the distribution below the thermal line while the latter, by removing the most eccentric stars, tends to push the distribution above the thermal line. For semi-major axes  $a = 1 - 3 \text{ mpc}$ , the IMBH lies almost completely within the orbits of the S-stars. Therefore, interactions only occur with the

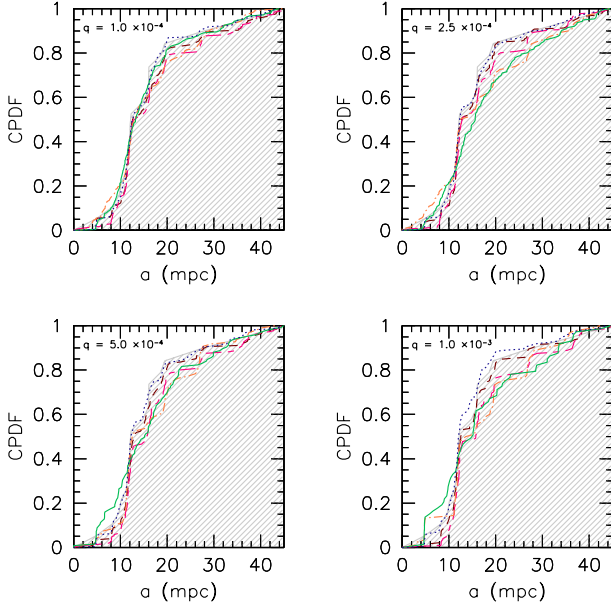


FIG. 12.— Cumulative distribution function for the semi-major axes of the S-stars after 10 Myr of evolution in the case of a circular binary. Line styles are as in Fig. 11.

stars that have small pericenter distances, leading to ejections. This is consistent with the fact that the most eccentric stars are the most likely to be ejected (see Fig. 7) as well as with the fact that the largest number of escapers is produced for  $a = 3$  mpc, regardless of the binary mass ratio (see Fig. 6). For  $a = 10$  mpc, the IMBH orbit intersects those of all the S-stars, thus resulting in strong perturbations on the orbital elements. The global increase in the eccentricities wins over the ejection of unbound stars in this case. The relative importance of escapers over the global perturbations on the orbital elements is also evident if we look at the mean eccentricity of the sample for a given binary mass ratio and initial separation. For  $a = 0.3$  and  $a = 30$  mpc, the value of the mean eccentricity  $\bar{e}$  remains close to that of the S-stars, which is  $\sim 0.75$ . For  $a = 1 - 3$  mpc, when ejections dominate, the mean eccentricity is reduced to  $\sim 0.6 - 0.65$ , while for 10 mpc  $\bar{e}$  achieves the largest value of  $\sim 0.8$ .

Figure 12 shows the cumulative distribution of the semi-major axes of bound stars at the end of the simulations. We limit the range of semi-major axes to 45 mpc, which is the maximum value observed in the current S-stars sample. Deviations from the observed distribution occur preferentially for large binary mass ratios and, in these cases, for binary separations in the range 3–10 mpc, similarly to what we observe for the eccentricity distributions.

Both Figure 11 and 12 show distributions after 10 Myr of integration. The evolution in the distributions, however, is expected to be time-dependent since the perturbations from the IMBH and the ejections tend to grow in time (see Fig. 8). We find that the effect of ejections becomes apparent after only 1–2 Myr and after 5 Myr the distributions take the form they have at the end of the simulations.

## 6. DISCUSSION

Our results help place limits on the orbital parameters of possible IMBHs in the Galactic center. Constraints have been placed in the past by several authors. One natural constraint

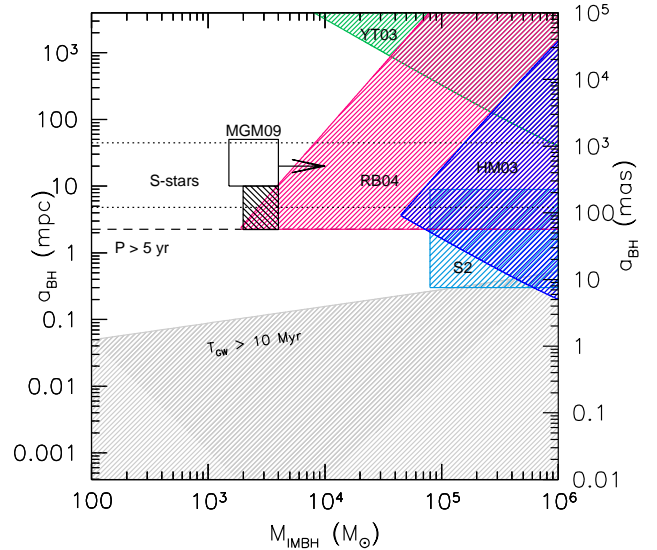


FIG. 13.— Constraints on the orbital parameters of a hypothetical IMBH in the Galactic region. The shaded areas represent regions of parameter space that can be excluded based on observational or theoretical arguments. The dotted lines mark the distances at which the S-stars are currently observed. The dashed line represents the 5 yr orbital period corresponding to discoverable systems. The parameters enclosed in the empty rectangular box are required for an efficient randomization of inclinations in the cluster infall scenario (Merritt et al. 2009). The small rectangular region just below the empty box represents the parameter space excluded by this work.

comes from the requirement that the center of mass of the binary coincides with the peak of the stellar distribution within the observational uncertainties (Yu & Tremaine 2003)

$$\frac{M_{\text{IMBH}}}{M_{\text{IMBH}} + M_{\text{SMBH}}} a_{\text{BH}} \lesssim 8 \text{ mpc}, \quad (17)$$

where  $a_{\text{BH}}$  represents the binary semi-major axis. The corresponding prohibited region in the  $M_{\text{IMBH}} - a_{\text{BH}}$  plane is shown in the upper right corner of Figure 13.

The orbit of a black hole binary shrinks due to emission of gravitational waves on a timescale given by Eq. 2. Demanding a lifetime of at least 10 Myr excludes the lowest region in Fig. 13 corresponding to small separations.

Gillessen et al. (2009) derive an upper limit of  $0.02 M_{\text{SMBH}}$  to the mass that can be contained within the orbit of star S2. This implies that no more than  $8 \times 10^4 M_{\odot}$  can be hidden between  $\sim 0.3$  mpc and  $\sim 9$  mpc of the SMBH.

The most stringent constraints can be derived from the astrometric wobble of the radio source SgrA\*, which could show indication of binary motion. Very Long Baseline Array observations from 1995 to 2000 show a residual motion for SgrA\* of  $\sim 0.5 \text{ mas} = 0.02 \text{ mpc}$  and an upper limit of  $\sim 8 \text{ km s}^{-1}$  for the peculiar motion perpendicular to the Galactic plane. Such limits exclude the rightmost triangular region in Fig. 13 (Hansen & Milosavljević 2003; Yu & Tremaine 2003). More recent measurements from Reid & Brunthaler (2004) find an upper limit to the motion in Galactic latitude of  $-0.4 \pm 0.9 \text{ km s}^{-1}$ . Combining this restriction with the 5 yr limit on observable systems results in the large triangle region in Fig. 13.

The perturbations exerted by an IMBH on the orbits of the S-stars allow us to exclude the region of parameter space corresponding to masses  $2000-4000 M_{\odot}$  and initial semi-major axes  $\sim 2-10$  mpc. Such region is represented by the shaded box in the figure.

Interestingly, the IMBH parameters required for an efficient randomization of inclinations (Merritt et al. 2009) in the cluster infall scenario ( $M_{\text{IMBH}} \gtrsim 1500 M_{\odot}$  for the simulated range of separations  $10-50$  mpc; see rectangular box in Fig. 13) are consistent with all the constraints placed so far. Mass ratios

larger than  $10^{-3}$  were not simulated but they are expected to operate even faster than the smaller ones.

We thank Douglas Heggie and Hagai Perets for useful discussions. This work was supported by grants AST-0206031, AST-0420920 and AST-0437519 from the NSF, grant NNG04GJ48G from NASA, and grant HST-AR-09519.01-A from STScI.

REFERENCES

Baumgardt, H., Gualandris, A., & Portegies Zwart, S. 2006, *MNRAS*, 372, 174

Binney, J., & Tremaine, S. 1987, *Galactic dynamics*, ed. J. Binney & S. Tremaine

Bonnell, I. A., & Rice, W. K. M. 2008, *Science*, 321, 1060

Brown, W. R., Geller, M. J., Kenyon, S. J., & Kurtz, M. J. 2005, *ApJ*, 622, L33

Eisenhauer, F., Genzel, R., Alexander, T., Abuter, R., Paumard, T., Ott, T., Gilbert, A., Gillessen, S., Horrobin, M., Trippe, S., Bonnet, H., Dumas, C., Hubin, N., Kaufer, A., Kissler-Patig, M., Monnet, G., Ströbele, S., Szeifert, T., Eckart, A., Schödel, R., & Zucker, S. 2005, *ApJ*, 628, 246

Figer, D. F. 2008, *ArXiv e-prints*

Genzel, R., Schödel, R., Ott, T., Eisenhauer, F., Hofmann, R., Lehnert, M., Eckart, A., Alexander, T., Sternberg, A., Lenzen, R., Clénet, Y., Lacombe, F., Rouan, D., Renzini, A., & Tacconi-Garman, L. E. 2003, *ApJ*, 594, 812

Gerhard, O. 2001, *ApJ*, 546, L39

Ghez, A. M., Duchêne, G., Matthews, K., Hornstein, S. D., Tanner, A., Larkin, J., Morris, M., Becklin, E. E., Salim, S., Kremenek, T., Thompson, D., Soifer, B. T., Neugebauer, G., & McLean, I. 2003, *ApJ*, 586, L127

Gillessen, S., Eisenhauer, F., Trippe, S., Alexander, T., Genzel, R., Martins, F., & Ott, T. 2009, *ApJ*, 692, 1075

Gould, A., & Quillen, A. C. 2003, *ApJ*, 592, 935

Hansen, B. M. S., & Milosavljević, M. 2003, *ApJ*, 593, L77

Harfst, S., Gualandris, A., Merritt, D., Spurzem, R., Portegies Zwart, S., & Berczik, P. 2007, *New Astronomy*, 12, 357

Heggie, D., & Hut, P. 2003, *The Gravitational Million-Body Problem: A Multidisciplinary Approach to Star Cluster Dynamics (The Gravitational Million-Body Problem: A Multidisciplinary Approach to Star Cluster Dynamics, by Douglas Heggie and Piet Hut. Cambridge University Press, 2003, 372 pp.)*

Kinoshita, H., & Nakai, H. 2007, *Celestial Mechanics and Dynamical Astronomy*, 98, 67

Kozai, Y. 1962, *AJ*, 67, 591

Löckmann, U., & Baumgardt, H. 2008, *MNRAS*, 384, 323

Martins, F., Gillessen, S., Eisenhauer, F., Genzel, R., Ott, T., & Trippe, S. 2008, *ApJ*, 672, L119

Matsubayashi, T., Makino, J., & Ebisuzaki, T. 2007, *ApJ*, 656, 879

Merritt, D., Gualandris, A., & Mikkola, S. 2009, *ApJ*, 693, L35

Mikkola, S., & Aarseth, S. J. 1993, *Celestial Mechanics and Dynamical Astronomy*, 57, 439

Mikkola, S., & Merritt, D. 2008, *AJ*, 135, 2398

Paumard, T., Genzel, R., Martins, F., Nayakshin, S., Beloborodov, A. M., Levin, Y., Trippe, S., Eisenhauer, F., Ott, T., Gillessen, S., Abuter, R., Cuadra, J., Alexander, T., & Sternberg, A. 2006, *ApJ*, 643, 1011

Perets, H. B., Gualandris, A., Kuzi, G., Merritt, D., & Alexander, T. 2009, *ArXiv e-prints*

Perets, H. B., Hopman, C., & Alexander, T. 2007, *ApJ*, 656, 709

Portegies Zwart, S. F., & McMillan, S. L. W. 2002, *ApJ*, 576, 899

Reid, M. J., & Brunthaler, A. 2004, *ApJ*, 616, 872

Spinnato, P. F., Fellhauer, M., & Portegies Zwart, S. F. 2003, *MNRAS*, 344, 22

Yu, Q., & Tremaine, S. 2003, *ApJ*, 599, 1129